AIP | Applied Physics Letters

Drift velocity peak and negative differential mobility in high field transport in graphene nanoribbons explained by numerical simulations

A. Betti, G. Fiori, and G. Iannaccone

Citation: Appl. Phys. Lett. **99**, 242108 (2011); doi: 10.1063/1.3664091
View online: http://dx.doi.org/10.1063/1.3664091
View Table of Contents: http://apl.aip.org/resource/1/APPLAB/v99/i24
Published by the American Institute of Physics.

Drift velocity peak and negative differential mobility in high field transport in graphene nanoribbons explained by numerical simulations

A. Betti,[a] G. Fiori, and G. Iannaccone
Dipartimento di Ingegneria dell'Informazione: Elettronica, Informatica, Telecomunicazioni, Università di Pisa, Via Caruso 16, I-56122 Pisa, Italy

(Received 9 August 2011; accepted 3 November 2011; published online 14 December 2011)

We present numerical simulations of high field transport in both suspended and deposited armchair graphene nanoribbon (A-GNR) on HfO_2 substrate. Drift velocity in suspended GNR does not saturate at high electric field (F), but rather decreases, showing a maximum for $F \approx 10$ kV/cm. Deposition on HfO_2 strongly degrades the drift velocity by up to a factor ≈ 10 with respect to suspended GNRs in the low-field regime, whereas at high fields, drift velocity approaches the intrinsic value expected in suspended GNRs. Even in the assumption of perfect edges, the obtained mobility is far behind what expected in two-dimensional graphene, and is further reduced by surface optical phonons. © *2011 American Institute of Physics*. [doi:10.1063/1.3664091]

Assessing the potential of graphene nanoribbons (GNRs) for future electronic applications requires full understanding of both quasi-equilibrium and far-from-equilibrium transport mechanisms.[1,2] However experimental low-field (LF) mobility in 1 nm-wide GNRs can be as low as ≈ 100 cm^2/Vs and is limited by edge disorder.[1,3] Furthermore, we know that achieving ideally smooth edges is not enough: full-band (FB) modeling shows that LF mobility due to only acoustic (AC) phonon scattering at low fields is close to 500 cm^2/Vs for 1 nm-wide GNRs.[4] Most importantly, nanoscale transistors do not operate in the LF mobility limit. Therefore, simulation of far-from-the-equilibrium transport conditions is required to understand achievable device performance. Whereas at low field, carrier scattering is mainly due to low-energy intravalley acoustic phonons,[4] at high electric field, scattering is dominated by optical phonon emission (EM), which becomes relevant when electrons gain enough energy to emit optical phonons. High-field steady-state transport can be simulated by solving the Boltzmann transport equation (BTE) through the single-particle Monte Carlo (MC) method. When dealing with 1D systems, however, particular attention has to be paid in accurately describing the energy dispersion relation due to quantum lateral confinement: for each GNR subband, there is a parabolic behavior close the subband minimum and then the typical graphene quasi-linear behavior already for relatively small wavevector values, corresponding to a velocity $\approx 8 \times 10^5$ m/s. Some authors have considered phonon confinement and multisubband transport, focusing on quantum wires with the effective mass approximation.[5,6] For GNRs, a multisubband MC approach has been followed in Ref. 7 and BTE has been solved in a deterministic way at criogenic temperatures in Ref. 8. Bresciani *et al.*[9] have used a 2D model, which is not fully adequate for sub-10 nm GNRs, where size effects are indeed relevant.

In this work, we adopt a steady-state single-particle full band MC approach accounting for carrier degeneracy,[10] which has a significant effect for materials with a small density of states as graphene. Scattering rates are obtained within the deformation potential approximation (DPA) from phonon dispersions described by means of the fourth-nearest-neighbour force-constant approach (4NNFC)[11] and a p_z tight-binding Hamiltonian for the electronic structure. We consider in-plane longitudinal acoustic and optical (LA and LO), transversal optical (TO), and surface optical (SO) phonons. In each subband, the rates are computed on a 2000-point grid in the k_x-space (due to symmetry, only longitudinal electron wavevectors $k_x > 0$ have been taken into account), considering energy up to 1.5 eV above the bottom of the first subband and including up to 18 subbands: this ensures accurate results even for strong longitudinal electric field $F \leq 3 \times 10^2$ kV/m and for all the considered GNR widths ($W \leq 10$ nm). Due to Van Hove singularities in the 1D rates, the self-scattering method[12] is inefficient, so that we have adopted the MC procedure described in Ref. 12 and extended to quasi-1D systems.[13] The whole story of an electron has a duration $T = \sum_i \Delta t_i$ ($T \leq$ (10–100) μs depending on W and F), where $\Delta t_i = t_{i+1} - t_i$ is the ith time step and t_i is the ith sampled time. At each t_i, the wavevector $\mathbf{k} = (k_x, k_{y\eta})$, where $k_{y\eta}$ is the transverse quantized electron wavevector,[4] is computed and the average value of quantity X (either the drift velocity $v(\mathbf{k}) = 1/\hbar \cdot \partial \mathrm{E}(\mathbf{k})/\partial k_x$ or the energy $E(\mathbf{k})$) is evaluated according to:[12] $\langle \mathrm{X} \rangle_t = \frac{1}{T}\int_0^T \mathrm{X}[k_x(t')]dt' = \frac{1}{T}\sum_{t_i}\int_{t_i}^{t_{i+1}} \mathrm{X}[k_x(t')]dt'$. The electronic temperature T_{el} under an applied homogeneous field F is computed by equating $\langle v(k_x)^2 \rangle$ with the mean squared velocity at equilibrium.[13] For $F = 0$, T_{el} is equal to the lattice room temperature T_{lat}, whereas for $F > 0$, $T_{el} > T_{lat}$. Once obtained T_{el}, the distribution function is updated accordingly at each t_i and final states for scattering are filled obeying to the Pauli exclusion principle (PEP).

The computed average drift velocity $\langle v_d \rangle$ limited by intrinsic phonons is plotted in Fig. 1(a) as a function of F for suspended sub-10 nm GNRs and for a carrier density $n_{2D} = 10^{12}$ cm^{-2}. $\langle v_d \rangle$ strongly varies within the considered F interval and a maximum appears at high electric field ($F = F_{th}$). For $F < F_{th}$, $\langle v_d \rangle$ can be fitted by means of the Caughey-Thomas model, i.e., $\langle v_d(F) \rangle = (\mu_{,0}F)/[1 + (\mu_{in,0}F/v_p)^{\gamma}]^{1/\gamma}$, where $\gamma \approx (1.3 \div 2)$, $\mu_{in,0}$ is the intrinsic LF mobility and v_p is the peak velocity, which ranges from 2×10^5 to 4×10^5 m/s, depending on W (Table I). $\langle v_d \rangle$ does not saturate with F, analogously to what has been observed in the case of

[a]Electronic mail: alessandro.betti@iet.unipi.it.

zigzag Carbon NanoTube (CNT).[14,15] As shown in Fig. 1(a), $\langle v_d \rangle$ slightly decreases for increasing F.[14] However, in constrast to Ref. 14, the negative differential mobility (NDM) cannot be explained by the increased number of populated states in the second subband with smaller $v(\mathbf{k})$. Indeed, as in Ref. 15, we have verified for $W = 10\,\text{nm}$ that such effect is much more pronounced if we fictitiously limit transport to only one subband (red dashed line in Fig. 1(a)). The velocity peak can be explained by the combined effect of the quasi-linear dispersion relation in GNRs and the strong increase of optical EM at high F, which increases the occurrence of back-scattering events, therefore, reducing the average velocity. If we follow the story of a single electron, we can see that as F increases, instantaneous electron velocity cannot increase beyond the limit imposed by the dispersion relation: any back-scattering event will invert the instantaneous velocity sign and, therefore, reduce the average velocity. Therefore, in the absence of optical phonon EM, the drift velocity $\langle v_d \rangle$ would saturate to about 8×10^5 m/s. The onset of optical phonon EM makes $\langle v_d \rangle$ peak at a fraction of that value and then decrease with F. We believe that the very same mechanism explains also the NDM in zigzag CNTs, as well as in graphene,[16] even if it has not been proposed before.[14,15] One can also see that the peak velocity v_p increases with W. Indeed, if $\hbar\omega$ is the optical phonon energy ($\approx$160 meV for LA mode), the current J can be estimated as $J = \frac{4e}{h}\hbar\omega\frac{E_F}{\pi\hbar v_F}$,[17] where v_F is the Fermi velocity. Since $v_p = J/(en_{2D})$ and the Fermi wavevector $k_F = \pi n_{2D} W$, we obtain $v_p = \omega \times W/\pi \propto W$.

The threshold field F_{th} strongly decreases with W, because of the increased mean free path $\langle L_{\mathbf{k}} \rangle$, which allows electrons to gain energy required to emit optical phonons at lower F. F_{th} can be roughly estimated by imposing the cutoff energy $\hbar\omega$ for optical EM equal to the mean kinetic energy gained between two scattering events, i.e., $qF_{th}\langle L_{\mathbf{k}} \rangle$. Since by increasing W from 1 to 10 nm, $\langle L_{\mathbf{k}} \rangle$ increases from $\approx$6 nm to 1 μm (Ref. 4) and F_{th} decreases from $\approx 2.7 \times 10^2$ kV/cm to $\approx$1.6 kV/cm. We remark also that the obtained values for $\langle v_{in} \rangle$ are in agreement with those found for zigzag CNTs with a circumference comparable with the considered W,

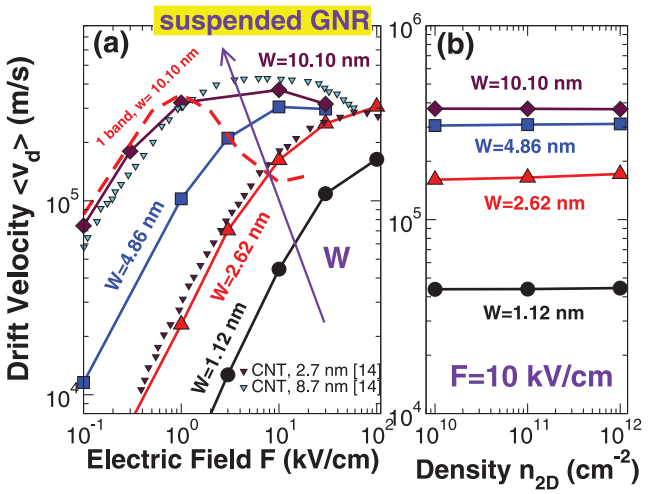

FIG. 1. (Color online) (a) Average drift velocity $\langle v_d \rangle$ as a function of F ($n_{2D} = 10^{12}\,\text{cm}^{-2}$) and (b) as a function of n_{2D} for different W of suspended GNRs. In (a), results from MC simulations for zigzag CNTs (Ref. 14) with sub-10 nm circumference (2.7 nm and 8.7 nm) are also reported. In (b), $F = 10$ kV/cm.

TABLE I. Caughey-Thomas parameters $\mu_{in,0}$, (cm^2/Vs), v_p (m/s) and γ for different W (nm), obtained through the fitting with MC data.

W	$\mu_{in,0}$	v_p	γ	W	$\mu_{in,0}$	v_p	γ
1.12	310	2.2×10^5	1.7	4.86	12000	3.3×10^5	1.4
2.62	2700	3.2×10^5	1.3	10.10	8000	3.7×10^5	2

both in linear and in non-linear regimes.[14] In Fig. 1(b), $\langle v_d \rangle$ is plotted as a function of n_{2D} for $F = 10$ kV/cm: $\langle v_d \rangle$ does not depend on n_{2D} even in the degenerate regime ($n_{2D} = 10^{12}\,\text{cm}^{-2}$), where the PEP limits up to the 50% of the scattering events. In Fig. 2, we show the intrinsic mobility $\mu_{in} \equiv \langle v_d \rangle / F$ as a function of F for $n_{2D} = 10^{12}\,\text{cm}^{-2}$. Since in the linear transport regime $v_d \propto F$, μ_{in} is constant for $F \leq F_{th}$ and decreases above F_{th} as $\mu_{in} \propto 1/F^{\alpha}$ with $\alpha > 1$. In addition, the narrower the ribbons, the stronger the suppression due to lateral confinement. Results are in good agreement with a multi-subband model for $W \approx 5$ nm.[7] In the inset of Fig. 2, the average kinetic electron energy $\langle E_{\mathbf{k}} \rangle$ in units of $k_B\,T_{lat}$ is shown as a function of F for $n_{2D} = 10^{12}\,\text{cm}^{-2}$. While for low $F \approx 0.1$ kV/cm electrons tend to remain near the first conduction subband edge and $\langle E_{\mathbf{k}} \rangle \approx 1/2\ k_B\,T_{lat}$ for the narrowest ribbons, for high field $F \geq 10^2$ kV/m, $\langle E_{\mathbf{k}} \rangle \gg k_B\,T_{lat}$ and higher energy states are occupied. Note also that $\langle E_{\mathbf{k}} \rangle$ increases with W, since subbands become closer, allowing electrons to populate higher subbands.

In Figs. 3(a) and 3(b), the average drift velocity $\langle v_d \rangle$ and the mobility $\mu_{ex} = \langle v_d \rangle / F$ are shown, respectively, as a function of F for GNRs deposited on HfO_2 (Ref. 4) including the effect of SO phonons ($n_{2D} = 10^{12}\,\text{cm}^{-2}$), through the first SO(1) and second SO(2) modes ($\hbar\omega_{SO} = 12.4$ meV for SO(1) mode). With respect to the suspended GNR case, $\langle v_d \rangle$, as well as mobility in GNR on HfO_2 are almost one order of magnitude smaller in the LF regime, while similar values are obtained for high field, as already noted for graphene on HfO_2.[16] As in graphene,[16] deposition on HfO_2 leads to an extension of the linear region to fields up to a factor 10 larger than those corresponding to suspended GNRs. For narrow ribbons, $\langle v_d \rangle$ does not saturate even for $F = 3 \times 10^2$ kV/cm.

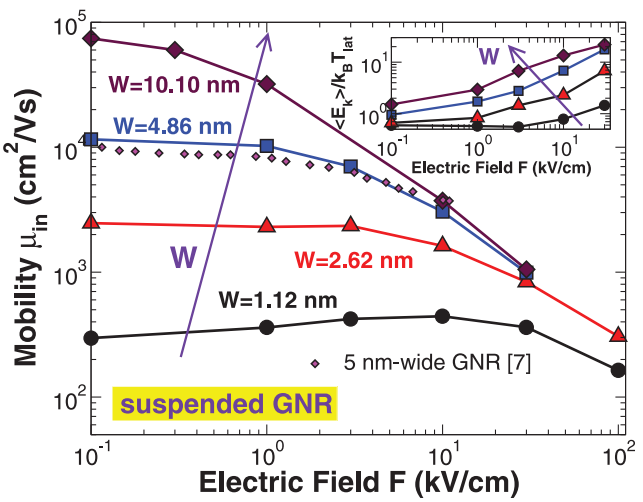

FIG. 2. (Color online) (a) Intrinsic mobility μ_{in} and (Inset) average kinetic electron energy as a function of F for different W. Results for GNRs with $W = 5$ nm (Ref. 7) are also shown in (a). $n_{2D} = 10^{12}\,\text{cm}^{-2}$.

In order to understand the different behaviour in suspended and deposited GNR on HfO_2, in Fig. 4(a), we show the distribution function G as a function of $(E_{\mathbf{k}} - E_{C1})$, where E_{C1} is the first subband edge, for $F = 1$ and 10 kV/cm ($W = 4.86$ nm) for GNRs, both suspended and deposited on HfO_2. At low fields, G decreases rapidly with energy in both cases, showing, unlike graphene, sharp peaks due to intersubband scattering. At high fields instead, electrons are excited up to energies close or above 1 eV, increasing T_{el} (inset of Fig. 2). As expected, deposition on HfO_2 leads to a shorter high energy tail compared to that in intrinsic GNR (Fig. 4(a)) due to the introduction of an additional channel for energy and momentum relaxation which increases total scattering rate and pushes electrons down to lower average electron energy. As for graphene on HfO_2,[16] the rough absence of degradation of $\langle v_d \rangle$ at high F can be explained by the reduced population in the high energy tail, i.e., by a smaller amount of electrons in the nonlinear dispersion energy region where the band velocity is smaller, which more than counterbalances the decrease of $\langle v_d \rangle$ resulting from the increased total scattering rate when depositing GNR on substrate. In order to explain the increase of the F interval, where $\langle v_d \rangle$ shows a linear behavior in the GNR on HfO_2 case, in Figs. 4(b) and 4(c), we show the relative ratio of scattering events for the different mechanisms as a function of F for 5 nm-wide suspended GNR and GNR on HfO_2, respectively. For intrinsic GNR and $F \leq 1$ kV/cm, the main scattering events involve absorption (ABS) and EM of LA phonons (Fig. 4(b)). For $F \geq 10$ kV/cm, optical phonon EM (of both LO and TO phonons) becomes predominant, increasing up to 30% of the total number of events. For GNR on HfO_2 instead, scattering involving SO(1) phonons happens very often already for $F = 1$ kV/cm whereas rates of LA, LO, and TO phonons are limited to few percents even for high fields, as can be seen in Fig. 4(c). In particular, the observed large absorption rate of SO(1) phonons (Fig. 4(c)), which is associated to the high Bose-Einstein occupation factor, appears to counterbalance SO(1) emission even at high F and is the responsible of the extension of the linear region up to fields of 10 kV/cm or above, depending on W.

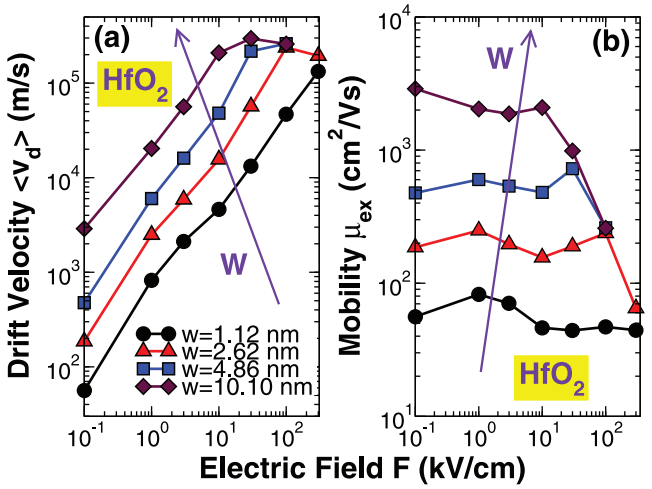

FIG. 3. (Color online) (a) Average drift velocity $\langle v_d \rangle$ and (b) mobility μ_{ex} as a function of F for GNR on HfO_2. $n_{2D} = 10^{12}$ cm^{-2}.

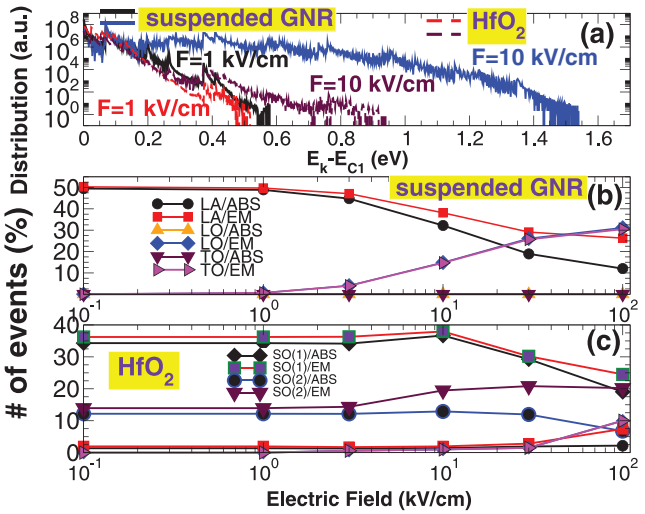

FIG. 4. (Color online) (a) Energy distribution function for $F = 1$ and 10 kV/cm for both suspended GNR (continuous lines, respectively) and GNR deposited on HfO_2 (dashed lines, respectively). Fraction of different scattering events as a function of F for (b) suspended GNR (LA, LO, and TO phonons) and (c) GNR deposited on HfO_2 (LA, LO, TO, and SO phonons). $W = 4.86$ nm and $n_{2D} = 10^{12}$ cm^{-2}.

In conclusion, we have performed a FB investigation of the dependence of drift velocity and mobility on the electric fields in GNRs. Suspended GNRs exhibit a drift velocity peak and then a NDM for large electric field, as also observed in zigzag CNTs. This property is due to the combined effect of quasi-linear dispersion relation and the emission of optical phonons. In particular, the maxima occur for a threshold field $F_{th} \propto 1/\langle L_{\mathbf{k}} \rangle \propto 1/W$. Depositing GNR on HfO_2 substrate strongly degrades $\langle v_d \rangle$ at low field by a factor $\approx$10, whereas at high fields, no degradation is observed.[16] Furthermore, in deposited GNRs velocity saturation and peak are shifted at higher F, due to the compensation of SO absorption and EM mechanisms.

Authors gratefully acknowledge support from the EU FP7 Project NANOSIL (No. 216171), GRAND (No. 215752) grants, and by the MIUR-PRIN project GRANFET (Project No. 2008S2CLJ9) via the IUNET consortium.

[1]X. Wang, Y. Ouyang, X. Li, H. Wang, J. Guo, and H. Dai, Phys. Rev. Lett. **100**, 206803 (2008).
[2]A. Betti, G. Fiori, and G. Iannaccone, IEEE Trans. Electron Devices **58**, 2824 (2011).
[3]Y. Yang and R. Murali, IEEE Electron Device Lett. **31**, 237 (2010).
[4]A. Betti, G. Fiori, and G. Iannaccone, Appl. Phys. Lett. **98**, 212111 (2011).
[5]S. Briggs and J. P. Leburton, Phys. Rev. B **38**, 8163 (1988).
[6]R. Mickevicius, V. V. Mitin, K. W. Kim, and M. A. Stroscio, Semicond. Sci. Technol. **7**, B299 (1992).
[7]L. Zeng, X. Y. Liu, G. Du, J. F. Kang, and R. Q. Han, in *International Conference on Simulation of Semiconductor Processes and Devices*, San Diego, CA (2009), pp. 1–4.
[8]D. Huang, G. Gumbs, and O. Roslyak, Phys. Rev. B **83**, 115405 (2011).
[9]M. Bresciani, P. Palestri, and D. Esseni, Solid-State Electron. **54**, 1015 (2010).
[10]P. Lugli and D. K. Ferry, IEEE Trans. Electron Devices **32**, 2431 (1985).
[11]R. Saito, G. Dresselhaus, and M. Dresselhaus, "Physical Properties of Carbon Nanotubes," (Imperial College Press, London, 2003).
[12]C. Jacoboni and L. Reggiani, Rev. Mod. Phys. **55**, 645 (1983).
[13]See supplementary material at http://dx.doi.org/10.1063/1.3664091.
[14]G. Pennington and N. Goldsman, Phys. Rev. B **68**, 045426 (2003).
[15]V. Perebeinos, J. Tersoff, and P. Avouris, Phys. Rev. Lett. **94**, 086802 (2005).
[16]X. Li, E. A. Barry, J. M. Zavada, M. B. Nardelli, and K. W. Kim, Appl. Phys. Lett. **97**, 232105 (2010).
[17]M. Freitag, M. Steiner, Y. Martin, V. Perebeinos, Z. Chen, J. C. Tsang, and P. Avouris, Nano Lett. **9**, 1883 (2009).